Liu *et al.*
Chinese Journal of Mechanical Engineering (2023) 36:28
https://doi.org/10.1186/s10033-023-00831-7

Chinese Journal of Mechanical Engineering

ORIGINAL ARTICLE

Open Access

Numerical Visualization of Grease Flow in a Gearbox

Hua Liu*, Florian Dangl, Thomas Lohner and Karsten Stahl

Abstract

Lubricating greases are widely used in e.g. open gear drives and gearboxes with difficult sealing conditions. The efficiency and heat balance of grease-lubricated gearboxes depend strongly on the lubrication mechanisms channeling and circulating, for which the grease flow is causal. The computational fluid dynamics opens up the possibility to visualize and understand the grease flow in gearboxes in more detail. In this study, a single-stage gearbox lubricated with an NLGI 1-2 grease was modeled by the finite-volume method to numerically investigate the fluid flow. Results show that the rotating gears influence the grease sump only locally around the gears. For a low grease fill volume, the rotation of the gears is widely separated from the grease sump. For a high grease fill volume, a pronounced gear-grease interaction results in a circulating grease flow around the gears. The simulated grease distributions show good accordance with high-speed camera recordings.

Keywords Lubrication, Grease, Transmission, Gearbox, Computational fluid dynamics

1 Introduction

Important aspects for the design of geared transmissions are noise-vibration-harshness behavior, load capacity, and efficiency. The last two aspects in particular greatly depend on the lubricant. Fluid lubrication can form a fluid film in e.g. gear and bearing contacts and supports heat dissipation. Fluid lubrication with liquids may refer to either oil or grease. Oil lubrication covers the majority of lubricant applications in gearboxes [1].

Grease lubrication can simplify the sealing design, as grease collars can assist with sealing. Moreover, grease tends to adhere to lubrication points. According to Schultheiss et al. [2], greases of low consistency numbers like NLGI 00 and 0 (DIN 51818 [3]) are typically used in the lubrication of open gear drives, e.g. in rotary furnaces or ball mills, whereas greases of higher consistency like NLGI 1 and 2 are typically applied to smaller gearboxes with difficult sealing conditions. Grease lubrication can achieve a long service life, and can be used for lifetime lubrication. The applicability of grease lubrication is typically limited to lower operating speeds and transmitted powers. This originates from its flow and lubrication characteristics (Section 2).

The application of computational fluid dynamics (CFD) has proven as helpful tool for understanding and assisting the lubrication design in gearboxes. Most studies have focused on oil lubrication, e.g. Liu et al. [4–8], Concli et al. [9–11], Kvist et al. [12] and Klier et al. [13]. In contrast to oil, grease exhibits a Bingham-like rheological behavior (Section 3).

There are only few CFD studies of grease flow. Concli et al. [11] modeled three lithium-soap greases of different consistency numbers flowing through a straight channel by means of a two-dimensional finite-volume based CFD model, using a single-phase Herschel-Bulkley rheology model. The numerical results in terms of velocity profiles closely match the experimental and analytical results, capturing the yield and shear-rate dependent characteristics of grease flow. Based on Ref. [14], Westerberg

*Correspondence:
Hua Liu
liu@fzg.mw.tum.de
School of Engineering & Design, Department of Mechanical Engineering, Technical University of Munich, Gear Research Center (FZG), Boltzmannstraße 15, 85748 Garching near Munich, Germany

et al. [15] modeled the grease flow in the grease pocket of a double-restriction seal geometry. Different rheological properties corresponding to NLGI 00, 1 and 2 greases, low and high rotational speeds as well as different temperatures were investigated. It was found that the flow and velocity distribution in the pocket is characterized by the rheological behavior of the grease. For high shear rates and temperatures, the grease approaches Newtonian behavior leading to reduced yield and shear-thinning characteristics. Klier et al. [13] conducted a single-phase CFD study on the laminar flow of greases in channels with rectangular cross section. A Herschel-Bulkley rheology model was applied. The numerical results are compared to both analytical results and flow measurements with particle image velocimetry. By means of a three-dimensional finite-volume based CFD model, Gertzos et al. [16] modeled the grease flow in a hydrodynamic journal bearing based on a Bingham rheology model. The performance characteristics such as relative eccentricity and pressure distribution are derived and presented for several geometries and shear rates. The results are found to be in good accordance with experimental and analytical data from previous investigations on Bingham fluids. Yoo and Kim [17] conducted numerical investigations on thermal elastohydrodynamically lubricated (EHL) line contacts with grease using a Herschel-Bulkley model. The results show that thermal effects play an important role especially at high rolling speeds and that the flow index and viscosity parameter of the Herschel-Bulkley model have a strong influence. Nogi et al. [18] investigated the grease film thickness in EHL point contacts numerically at low speeds. Recently, Mastrone and Concli [19] applied a CFD model to investigate the fluid flow and no-load gear power loss of a NLGI 1 grease in a test gearbox of the FZG back-to-back test rig. Thereby, grease fill volumes of 40%, 50% and 80% were investigated at medium circumferential speed.

In this study, a finite-volume (FV) based CFD model of a single-stage gearbox lubricated with an NLGI 1-2 grease was built to investigate the fluid flow. The measured grease rheology is described by a modified Bingham model. Three different grease fill volumes as well as two circumferential speeds are considered. The numerical results are discussed to identify grease flow phenomena in gearboxes. Validation is obtained by means of high-speed camera recordings.

2 Grease Lubrication in Gearboxes

For grease-lubricated gearboxes, circulating and channeling were identified as two main gear lubrication mechanisms (Fukunaga [20], Hochmann [21], Stemplinger [22]).

Channeling refers to certain operating conditions with only very little interaction of gears with grease, see Figure 1 (left). The gears rotate in an almost grease-free volume with a gap to the surrounding grease. No fresh grease from the grease sump flows and interacts with the gears. Lubrication of the gear mesh is only provided by from the grease separated oil accumulating below the gears. Channeling results in poor lubrication and heat dissipation, and mainly occurs for lower grease fill volumes and higher NLGI numbers. Circulating refers to certain operating conditions with relevant interaction of gears with grease, see Figure 1 (right). Grease around the gears follows the rotational movements of the gears and interacts with the gears. Grease closer to the housing of the gearbox remains static. Circulating provides good lubrication and supports heat dissipation. It mainly occurs for higher grease fill volumes.

There is no general design criterion to predict the resulting lubrication mechanism of grease-lubricated gearboxes. It strongly depends on the temperature, grease fill volume, load, speed and grease composition [22].

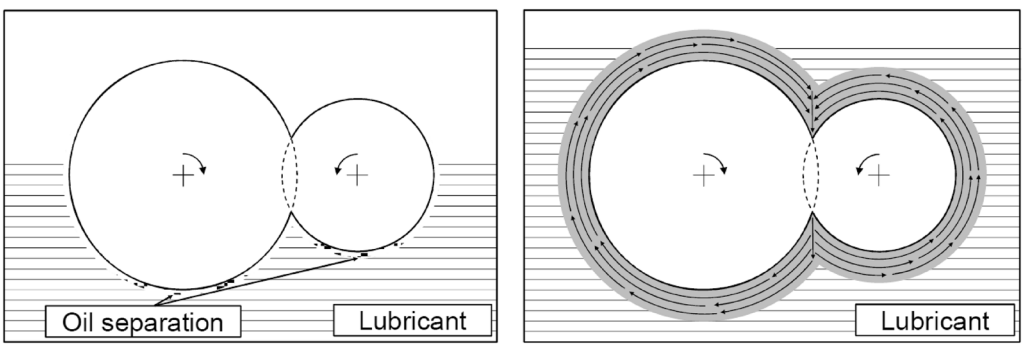

Figure 1 Schematic illustration of channeling (left) and circulating (right) as main lubrication mechanisms of grease-lubricated gearboxes [22, 23]

Stemplinger [22] performed experiments with a single-stage test gearbox at the FZG back-to-back test rig. He found that for grease fill volumes of 40 and 50%, channeling dominates. For a grease fill volume of 80%, circulating predominates. A grease fill volume of 50% is suggested as compromise between acceptable no-load gear losses and sufficient lubrication and heat dissipation. Further experimental investigations of Stemplinger [22] show that the speed has a strong impact on the lubrication mechanism. At low circumferential speeds, circulating tends to be dominant. With higher circumferential speeds, channeling becomes dominant. This is confirmed for small module gears by Schultheiß [24]. Siewerin et al. [25] show a strong influence of temperature on the lubrication supply mechanism. For NGLI 1 greases, circulating is more supported for a sump temperature of 90 °C than 60 °C.

The thickener also influences the lubrication mechanism. Fukunaga [20] states that the consistency is more important than the base oil viscosity. He shows that lithium- and aluminum-complex soap thickeners have the best phase separation, which is advantageous for oil separation from the grease and hence for both channeling and circulating. A calcium complex soap thickener tends to promote channeling. Combined with limited phase separation capability, it leads to a poor grease supply of the gear mesh. Fischer et al. [26, 27] point out that the base oil type of a grease can strongly affect lubricant film formation in EHL contacts. The presence of a thickener layer can separate the contacting surfaces under starved lubrication.

Grease lubrication in gearboxes depends on a large number of influencing factors, which affect the efficiency, heat dissipation and load capacity. Essential is the occurrence of channeling or circulating as lubrication mechanism, for which the grease flow behavior is causal. Based on an appropriate rheology model, the application of CFD can provide insights into grease flow phenomena in gearboxes.

3 Rheology of Greases

The rheological behavior of fluids can be divided in Newtonian or non-Newtonian [28]. Figure 2 gives an overview of different rheological behaviors. The shear stress τ of Newtonian fluids (a) is proportional to the shear rate $\dot{\gamma}$, with the dynamic viscosity η as a constant of proportionality:

$$\tau = \eta \cdot \dot{\gamma}. \tag{1}$$

The viscosity of non-Newtonian fluids depends on the shear rate. A fluid with increasing viscosity with increasing shear rate (shear thickening) is called dilatant (c). A fluid with decreasing viscosity with increasing shear rate (shear thinning) is called pseudoplastic (b). Bingham fluids (d, e) show a yield stress τ_0. Fluid flow only occurs when the external stresses are larger than the yield stress. The behavior can then be plastic (d) or pseudoplastic (e). Moreover, the rheological behavior may be

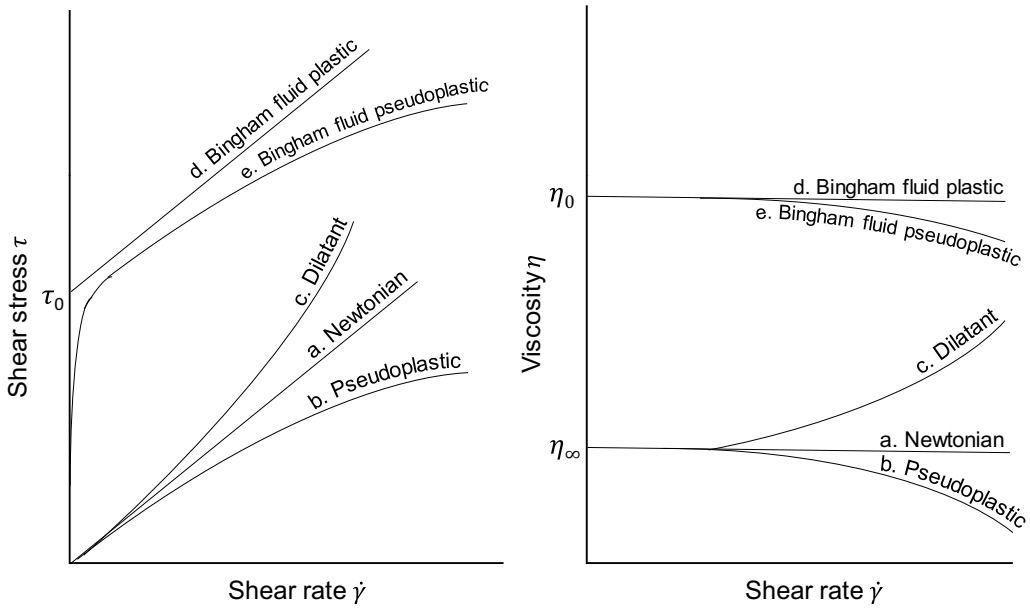

Figure 2 Schematic representation of different rheological behavior of fluids (based on Ref. [28])

time-dependent with increasing viscosity (rheopexic) and decreasing viscosity (thixotropic). Viscoelastic fluids have elastic and viscous properties.

Oils show typically a pseudoplastic (b) behavior at high pressure and shear rate. In the context of gearbox oil flow, it can be considered as Newtonian. Conversely, greases display Bingham-like behavior (d, e). Due to the thickener, they behave like elastic solid materials as long as the external stress is below the yield stress. When the yield stress is exceeded, it starts to flow. Thereby, a plastic behavior (d) with constant viscosity or a pseudoplastic behavior (e) with decreasing viscosity and increasing shear rate can occur.

4 Methodology

This section describes the considered gearbox, grease and operating conditions as well as the developed CFD model and the calculation and experimental procedure.

4.1 Gearbox

The considered test gearbox features the same geometry as considered in previous studies (Liu et al. [4, 5, 7]). It has a width of 260 mm, a height of 171 mm and a depth of 56 mm. The front cover is made of acryl glass, which allows optical accessibility of the grease distribution. Figure 3 shows the test gearbox filled with the considered grease (Section 4.2) without front and top cover. The considered test pinion and wheel are of FZG type C-PT as used in Refs. [4, 5, 7]. The main geometry data is shown in Table 1.

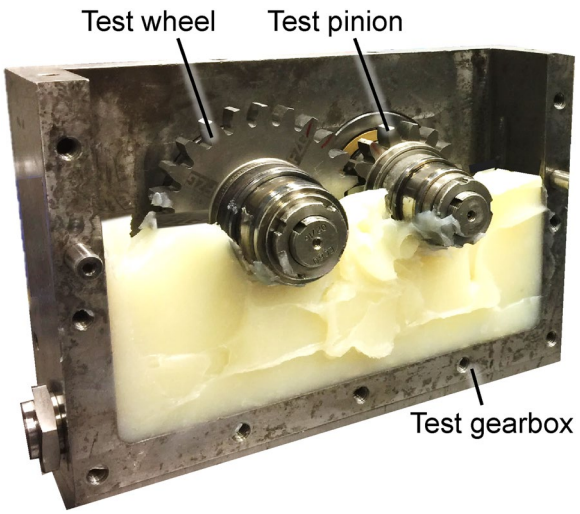

Figure 3 Considered test gearbox (without front and top cover)

4.2 Grease

A NLGI 1-2 grease with measured rheology data according to Table 2 is considered [29]. The grease was sheared at 1000 1/s and 25 °C. After that, its viscosity was measured at different shear rates. The base oil was extracted from the grease and measured separately. For each shear rate, an arithmetic mean value of the viscosity was derived from ten single measurements.

The grease shows a clear dependency of the viscosity on the shear rate, whereas the viscosity of the base oil is independent of the shear rate.

4.3 Operating Conditions

In accordance with the main influencing factors on the grease lubrication mechanisms (Section 2), the grease fill volume and the circumferential speed are varied. Based on investigations of Refs. [22, 25], the circumferential speeds of $v_t = \{0.05; 0.38\}$ m/s and the grease fill volumes of 40 %, 54% and 80% are considered according to Table 3. Thereby, the wheel in Figure 3 rotates clockwise and the pinion counter-clockwise. The present secondary medium in the gearbox is air.

Table 2 Measured shear rate and viscosity for the considered grease and its base oil at 25 °C

Shear rate $\dot{\gamma}$ (1/s)	Viscosity η (mPas) Grease	Viscosity η (mPas) Base oil
0.1	2,012,170.00	49.74
1	176,862.50	49.74
10	47,838.20	49.74
100	6864.04	49.74
1000	1163.52	49.74
10,000	262.06	49.74
15,000	220.27	49.74

Table 1 Main geometry data of the considered test gears of FZG type C-PT

	a(mm)	$z_{1\|2}$	m_n (mm)	α_n (°)	$x_{1\|2}$ (mm)	$b_{1\|2}$ (mm)	$d_{a1\|2}$ (mm)
Pinion (1)	91.5	16	4.5	20.0	0.182	14	82.5
Wheel (2)		24			0.171		118.4

Table 3 Considered operating conditions

Rotational speed of pinion n_1 (r/min)	Circumferential speed v_t (m/s)	Grease fill volume (%)	Grease temperature (°C)
13	0.05	40	25
100	0.38		
13	0.05	54	
100	0.38		
13	0.05	80	
100	0.38		

Table 4 Specializations of the generalized conservation equation [30]

	Φ	D_Φ	Q_Φ
Mass conservation	1	0	0
Impulse conservation	$\overline{u}$	$\nabla \cdot \overline{\tau}$	$-\nabla p + \eta \Delta \overline{u} + \rho \overline{g} + F$
Energy conservation	h	$-\nabla \cdot \overline{q''}$	$\frac{\partial p}{\partial t} + \nabla \cdot (\overline{\tau} \cdot \overline{u})$

4.4 Numerical Model

The numerical model is implemented and solved using the commercial CFD software Ansys Fluent 19.0. The Eulerian FV based method is applied. By solving the conservation equations, state variables like pressure, density and velocity of the medium can be determined at every position and every time within the domain.

4.4.1 Governing Equations

The Navier-Stokes equations are a compilation of conservation equations with respect to mass, impulse and energy. A generalized form of the conservation equations is shown in Eq. (2) [30] with the specializations shown in Table 4. Depending on the variables substituted in this equation, different forms of conservation result.

$$\underbrace{\frac{\partial}{\partial t}(\rho\Phi)}_{\text{local temporal change within CV}} + \underbrace{\underbrace{\Delta(\rho\overline{u}\Phi)}_{F_\Phi}}_{\text{Convective flow across the border of CV}} - \underbrace{\underbrace{\nabla \cdot (\Gamma \nabla \Phi)}_{D_\Phi}}_{\text{diffusive flow across the border of CV}} = \underbrace{Q_\Phi}_{\text{sources}}. \tag{2}$$

By means of Eq. (2), an arbitrary state variable can be substituted for Φ. The first summand on the left-hand side describes the partial derivation of the state variable. It describes the change in the state variable over time. The second summand on the left-hand side represents the transport of flow information, which is known as the convective part of the state variable. The first summand on the right-hand side of the equation represents the transport of flow by random flow motion, which indicates the diffusive part of flow, whereas the second summand on the right-hand side represents the different types of sources.

There are only very few simple flow configurations, such as the direct flow against the cylinder, which can be described by analytical equations. If the problem becomes more complex, numerical methods are required to solve these conservation equations. Thereby, the conservation equations are transformed into a differential or integral form. The integral form known as the FV method is a common form for solving fluid mechanical problems due to its conservative character, which means that the state variables are conserved even after derivation. By applying the Gaussian Integral, Eq. (2) reads as follows:

$$\int_{\mathrm{CV}} \frac{\partial}{\partial t}(\rho\phi)\mathrm{d}V + \oint_{\mathrm{SF}} \left(\vec{u}\,\rho\phi\right) \cdot \vec{n}\,\mathrm{d}A - \oint_{\mathrm{SF}} (\Gamma\nabla\phi) \cdot \vec{n}\,\mathrm{d}A = \int_{\mathrm{CV}} Q_\phi \mathrm{d}V, \tag{3}$$

where CV and SF indicate the control volume and its surface. By summing up the surface integral of the entire control volumes, the surface integrals of the inner control volumes cancel each other out, whereas the surface integrals of the outer control volumes remain in the system.

The conservation equations in integral form are solved by numerical approximation. First, the integrals are approximated by Gauss quadrature as function at one or a couple of points on the border of the control volumes. Second, the values on these points are determined by interpolation with known values in adjacent control volumes. Third, the derivations are replaced and solved by finite differences on the different integration points. The accuracy of the numerical approximation increases with the order of interpolation and the fineness of discretization.

For multiphase problems with immiscible fluids, the Volume of Fluid (VoF) method is applied. Thereby, the fluid variables in each finite volume either originate from a single phase, or from a mixture of phases, depending on the volume fraction α in each finite volume [19, 31]. For the density ρ, it reads:

$$\rho = \alpha\rho_q + (1-\alpha)\rho_p. \tag{4}$$

The conservative form of the scalar advection equation for the volume fraction α can be written as:

$$\frac{d\alpha}{dt} = \frac{\partial\alpha}{\partial t} + u_i\frac{\partial\alpha}{\partial x_i} = 0, \tag{5}$$

$$\frac{\partial \alpha}{\partial t} + \nabla(\alpha \vec{U}) = 0. \tag{6}$$

Eq. (6) is integrated over control volumes and a time interval δ_t with finite volume method. By applying the Gauss integral, Eq. (6) leads to:

$$\int_{\mathrm{t}}^{\mathrm{t}+\delta\mathrm{t}} \left(\int_{\mathrm{KV}} \frac{\partial \alpha}{\partial t} \mathrm{dV} \right) \mathrm{d}t + \int_{\mathrm{t}}^{\mathrm{t}+\delta\mathrm{t}} \left(\int_{\mathrm{KV}} \nabla(\alpha \vec{U}) \mathrm{d}V \right) \mathrm{d}t = 0. \tag{7}$$

By using the Gauss quadrature, Eq. (7) for the volume fraction α becomes a bunch of linear equations, which can be solved numerically, whereas P indicates the center of the control volume and f represents the centroid of its border:

$$(\alpha_P^{t+\delta\mathrm{t}} - \alpha_P^{\mathrm{t}}) V_P + \sum_{f=1}^{n} \left[(1-\eta) \left(\alpha_f \vec{U_f} \vec{A_f} \right)^t + \eta \left(\alpha_f \vec{U_f} \vec{A_f} \right)^{t+\delta\mathrm{t}} \right] \delta\mathrm{t} = 0. \tag{8}$$

According to the discretization scheme, η can be set to 0 for Euler explicit, 1 for Euler implicit or $\frac{1}{2}$ for Crank-Nicholson scheme.

After solving the variable for the volume fraction α, the continuity equation for each phase in each control volume can be described as:

$$\frac{\partial(\alpha_q \rho_q)}{\partial t} + \nabla(\alpha_q \rho_q u_q) = S_{\alpha_q} + \sum_{p=1}^{n} (\dot{m}_{pq} - \dot{m}_{qp}). \tag{9}$$

As described before, after Eq. (9) is transformed into integral form, the domain is discretized and the integrals are decoupled by Gaussian quadrature in its implicit scheme:

$$\frac{(\alpha_q^{n+1} \rho_q^{n+1} - \alpha_q^n \rho_q^n)}{\Delta t} V + \sum_f (\rho_q^{n+1} U_f^{n+1} \alpha_{q,f}^{n+1}) = \left[S_{\alpha_q} + \sum_{p=1}^{n+1} (\dot{m}_{pq} - \dot{m}_{qp}) \right]. \tag{10}$$

After determining the volume fraction in each control volume, the conservation equations for momentum are solved with the averaged fluid variables in a joint momentum equation through all control volumes in the domain.

The fluids are considered as compressible. Thermal influences are neglected and therefore the energy conservation equation is not considered.

A pressure-velocity coupled scheme based on algorithm SIMPLE is used, whereas the momentum equations are discretized by second order upwind. The VoF equations are interpolated by a downwind compressive scheme, which is able to preserve a good resolution for the interfaces between the phases even with coarse meshes or high Courant numbers. Turbulence models are not applied in this study due to small Reynolds numbers (Section 4.4.4).

4.4.2 Rheological Model

The rheological behavior of a grease can be described as Bingham-like behavior (Section 3), for which several models are available to describe the relationship between shear stress, shear rate and viscosity. In this study, a modified Bingham model is used [29].

The classical Bingham plastic model can be seen as a special form of the Herschel-Bulkley model [32]. As long as the stress does not exceed the yield stress ($\tau < \tau_0$), the grease behaves like an elastic solid body.

When the yield stress is exceeded ($\tau > \tau_0$), it shows a linear behavior and reads [28]:

$$\tau = \tau_0 + \eta_{BH} \dot{\gamma}. \tag{11}$$

Thereby, τ_0 denotes the yield stress and η_{BH} the Bingham viscosity. Eq. (11) can also be written in terms of viscosity:

$$\eta = \eta_{BH} + \frac{\tau_0}{\dot{\gamma}}. \tag{12}$$

A modified Bingham model is obtained by introducing the exponent n and interpreting the Bingham viscosity as the base oil viscosity of the grease η_{Oil}:

$$\eta = \eta_{oil} + \frac{\tau_0}{\dot{\gamma}^n}. \tag{13}$$

Based on the measured relationship of shear rate and viscosity of the considered grease (Table 2), the modified Bingham model can be parameterized by regression analysis. Figure 4 illustrates the measured and predicted shear stress

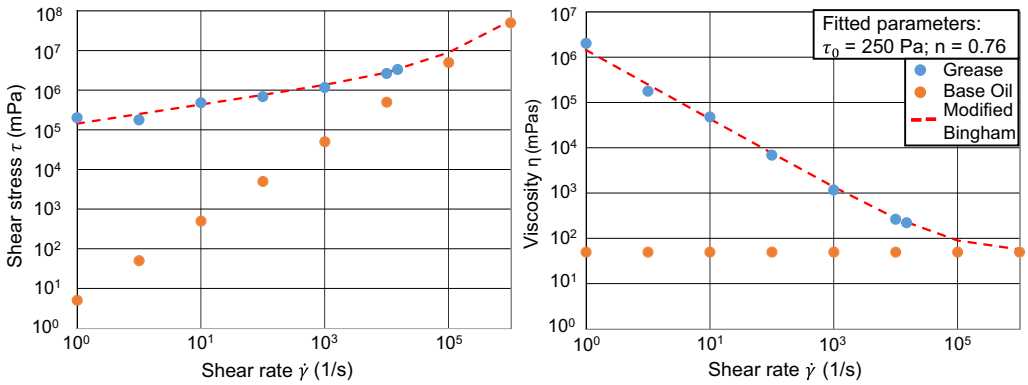

Figure 4 Measured and predicted relationship between shear stress and shear rate (left) and viscosity and shear rate (right) of the considered grease

and viscosity over shear rate. Based on the fitted parameters $\tau_0 = 250$ Pa and $n = 0.76$, very good correlation is found.

The modified Bingham model is implemented in the simulation model by compiling a user-defined material property function. Depending on the kinematics of the test gears and the shear rate $\dot{\gamma}$, the non-linear grease viscosity η will be calculated for each time step and position in the flow domain. It is used as an input variable for the conservation equations. Compared to oil flow simulations based on Newtonian fluids, this implicit calculation of viscosity requires more computational effort.

4.4.3 Model Description

The conservation equations are solved iteratively for both phases within the finite volumes in the flow domain (Section 4.4.1). Therefore, a discretization of the flow domain is required.

According to Figure 5 (top), the geometry of the considered test gearbox (Figure 3) is prepared by focusing

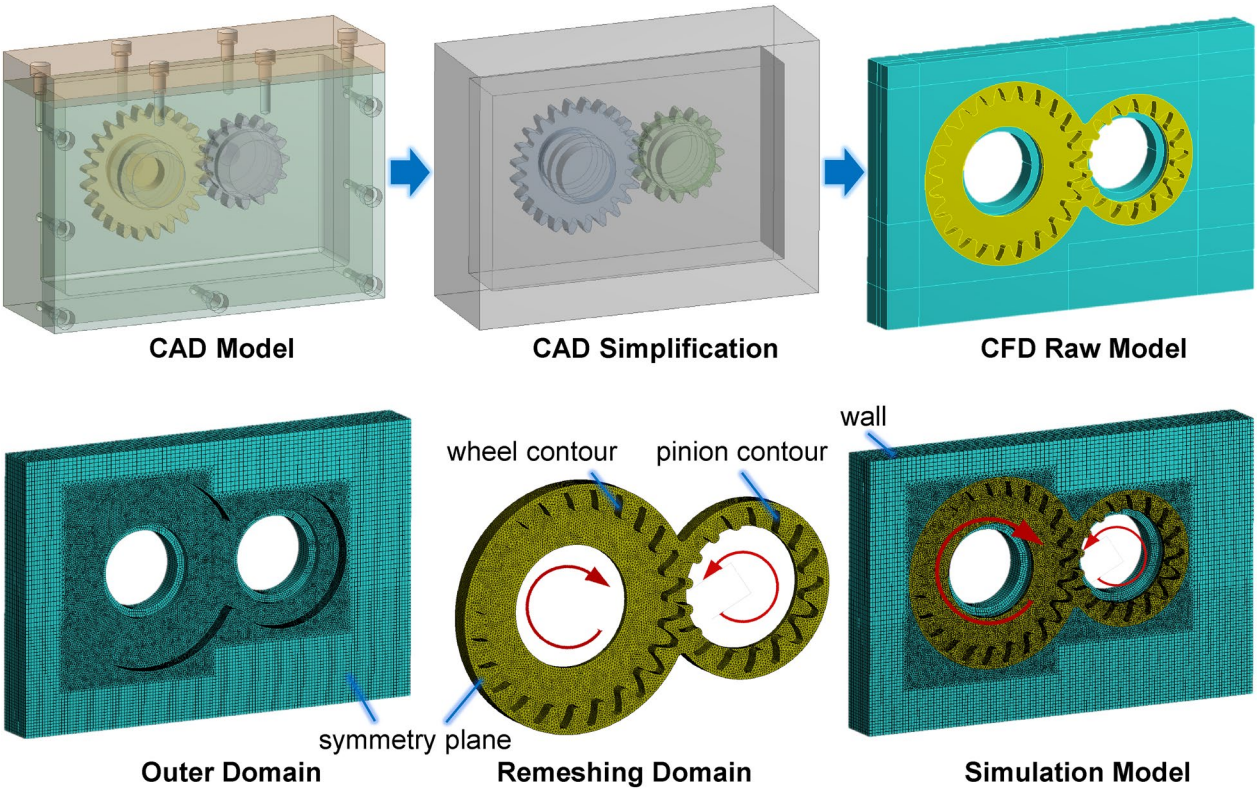

Figure 5 Derivation of CFD simulation model from CAD model

on the geometry relevant for fluid flow. Components like screws and dowel pins, as well as small housing curvatures, are neglected. The whole geometry is then subtracted from a cuboid, so that a negative raw model of the test gearbox is created. Due to the symmetry of the test gearbox, only one half is modeled, while the middle plane of the test gearbox is set to symmetry boundary condition.

Figure 5 (bottom) shows the mesh model of the considered test gearbox, which has been already considered and generally explained by the authors in Ref. [7]. Some descriptions on the mesh model are repeated to improve readability. The mesh model is divided into two domains, which are connected with each other sharing the same grid points: the outer domain and the remeshing domain. The outer domain is mainly discretized by hexahedral elements and remains static, whereas the contours of pinion and wheel of the remeshing domain rotate at a predefined speed. The remeshing domain is used to balance out the mesh deformation caused by the gear kinematics. It consists of a deformable meshing structure with tetrahedral elements, which are stretched or rebuilt with every time step. When the mesh quality, evaluated by e.g. skewness and orthogonal quality, falls below a minimum mesh quality, the affected elements are reconstructed. Due to the very small gap between the tooth flanks, i.e. gear backlash, bad element quality and numerical singularities would occur during numerical analysis. Therefore, the pinion and the wheel are scaled to 98% of their actual size. The scaling is not expected to significantly influence the predicted grease distribution.

The element grid size is selected based on a grid sensibility analysis in Ref. [5]. In the outer domain it is between 2.0 and 3.0 mm, whereas in the remeshing domain it is set to 1.25 mm, resulting in a total element number of 0.7 M. Although the fluid flow can be resolved better with higher element numbers, the element grid size chosen is a compromise between resolution and computing effort.

Adhesion and surface tension usually becomes important when the gravitation or exterior force is near-zero. In this study, the adhesion angle between both phases is set to 90° at walls, from which the adhesion force is derived.

Further details in terms of modeling can be found in previous studies [5, 7, 8].

4.4.4 Calculation Procedure

The described numerical model is used to investigate the fluid flow behavior in the considered grease-lubricated gearbox for different grease fill volumes and circumferential speeds.

As the numerical model starts from a motionless state, an acceleration ramp with a physical acceleration time of 0.125 s is applied to ensure physical plausibility and numerical stability. The time steps are set to 1.28 ms and 0.67 ms, which equals 0.1° rotation of the pinion at $n_1 = 13$ r/min and $n_1 = 100$ r/min (Table 3). The CFL number at these time steps is 0.05, which is much lower than 1 and assures numerical stability [33]. A local convergence criterion of 10^{-5} is used for all equations. A global convergence criterion of 10^{-3} complies for every time step.

The global Reynolds number can be estimated by $Re = \frac{\omega r_P^2}{\nu}$ and is << 1 for the considered operating conditions. The local cell Reynolds number as the ratio of local inertia and viscous force $Re = \frac{\rho u L}{\eta}$ is mostly < 1. The maximum local cell Reynolds numbers appear in air phase around the gears and is << 100. This indicates that the considered mesh size is suitable.

All calculations were conducted at the Leibnitz Rechenzentrum (LRZ). 28 cores (Intel Xeon E5-2690 v3 @ 2.6 GHz) and 64 Gb Ram were used. The simulations were carried out with the commercial software Ansys Fluent (Release 2018 R1). The required calculation time for the simulation of one wheel rotation was in average approximately 20.5 h.

4.4.5 Experimental Procedure

For validation of the numerical results, the considered test gearbox (Section 4.1) is investigated at a FZG back-to-back test rig according to ISO 14635-1 [34]. The grease distribution was captured for all investigated operating conditions by means of a high-speed camera running at 3000 fps. Before each recording, the gears were cleaned from grease and the initial grease fill volume was carefully adjusted for each measurement. It should be noted that the exact grease fill volume is difficult to implement due to the consistency of the grease.

5 Results and Discussion

In this section, numerical results on the grease distribution are discussed and compared with high-speed camera recordings. In Section 5.1, the grease distribution is analyzed during the first wheel rotation. This provides insights into the initial grease removal from the grease sump and its transport to the gear mesh. The subsequent evaluation of the grease distribution after four wheel rotations in Section 5.2 allows interpretation on grease flow phenomena after several grease exchange in the gear mesh has taken place several times. In Section 5.3, the trend of grease fraction near the pinion and wheel is evaluated in order to quantify the presence of grease for lubrication of the gear mesh.

5.1 Grease Distribution during First Wheel Rotation

Figure 6 compares the simulated grease distribution with high-speed camera recordings for grease fill volumes of 40%, 54% and 80% at one-quarter, one-half, and three-quarter wheel rotation. For simplicity, the circumferential speed of $v_t = 0.05$ m/s is considered, as the grease distribution during the first wheel rotation for $v_t = 0.38$ m/s behaves very similar. Note that camera recordings are shown from the front view on the gearbox, whereas the simulation results are illustrated in a slightly angled view to increase information transfer.

The area of pinion and wheel initially covered with grease in the sump depends on the grease fill volume before start-up. It is larger for higher grease fill volumes.

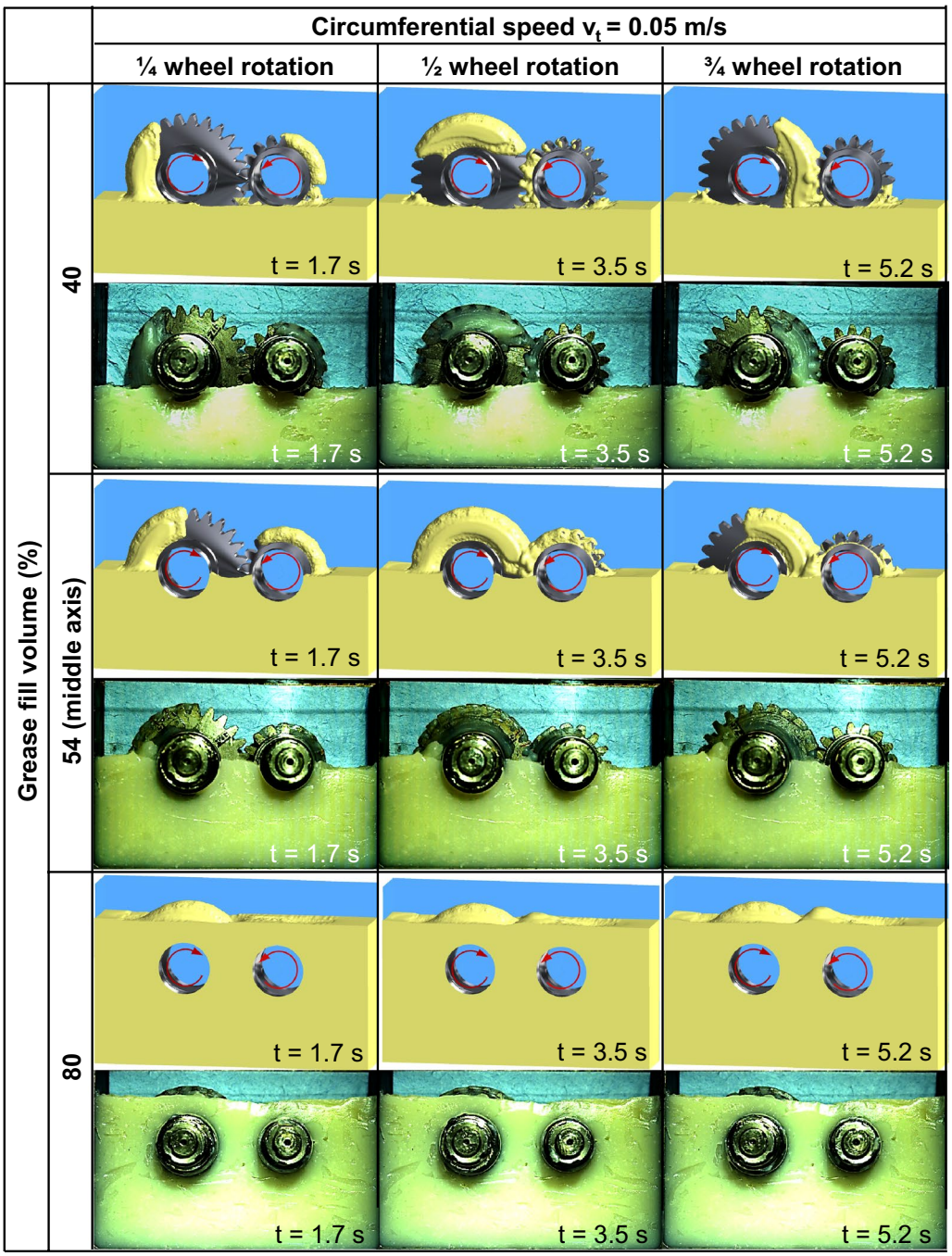

Figure 6 Simulated and recorded grease distributions for circumferential speed v_t of 0.05 m/s and grease fill volumes of 40%, 54% and 80% at one-quarter, one-half, and three-quarter wheel rotation

When the gears start to rotate, the grease is dragged out of the grease sump as it sticks in the tooth gaps and at the gear face (cf. one-quarter of wheel rotation).

For the grease fill volume of 40%, the absent grease back flow to the sump is clearly recognized after one-half of wheel rotation. The initially grease-free gear areas have rotated through the grease sump without picking up further grease. Hence, no interaction with grease has taken place, as the grease in the sump behaves like an elastic solid body. After three-quarter of wheel rotation, the dragged grease by the wheel interacts with the pinion in the gear mesh. For the grease fill volume of 54%, larger gear areas are initially covered with grease. Dragged grease by the gears already interacts after one-half of wheel rotation. Hence, the time share of grease exchange between the pinion and wheel in the gear mesh increases. For the grease fill volume of 80%, the pinion is fully covered with grease and only a small part of the wheel protrudes from the grease sump. The small part of the wheel that was initially uncovered cannot be seen at one-quarter, one-half and three-quarter wheel rotation in Figure 6.

The degree of grease coverage of gears correlates qualitatively well between simulation results and high-speed camera recordings. For the grease fill volume of 80%, the bead above the gear mesh predicted by the simulation is not found experimentally. The bead becomes more pronounced after four wheel rotations (Section 5.2).

The results during the first wheel rotation of the grease-lubricated gear stage show a very limited backflow of grease to the gear areas in the sump. Mainly the interaction of initially with grease covered pinion and wheel areas in the gear mesh supports the grease flow and distribution.

5.2 Grease Distribution after Four Wheel Rotations

Figure 7 shows the simulated and recorded grease distributions after four wheel rotations for the considered operating conditions in Table 3. The three columns correspond to the grease fill volumes of 40%, 54% and 80%, whereas the two rows relate to the circumferential speeds v_t of 0.05 m/s and 0.38 m/s. Note that camera recordings are shown from the front view on the gearbox, whereas

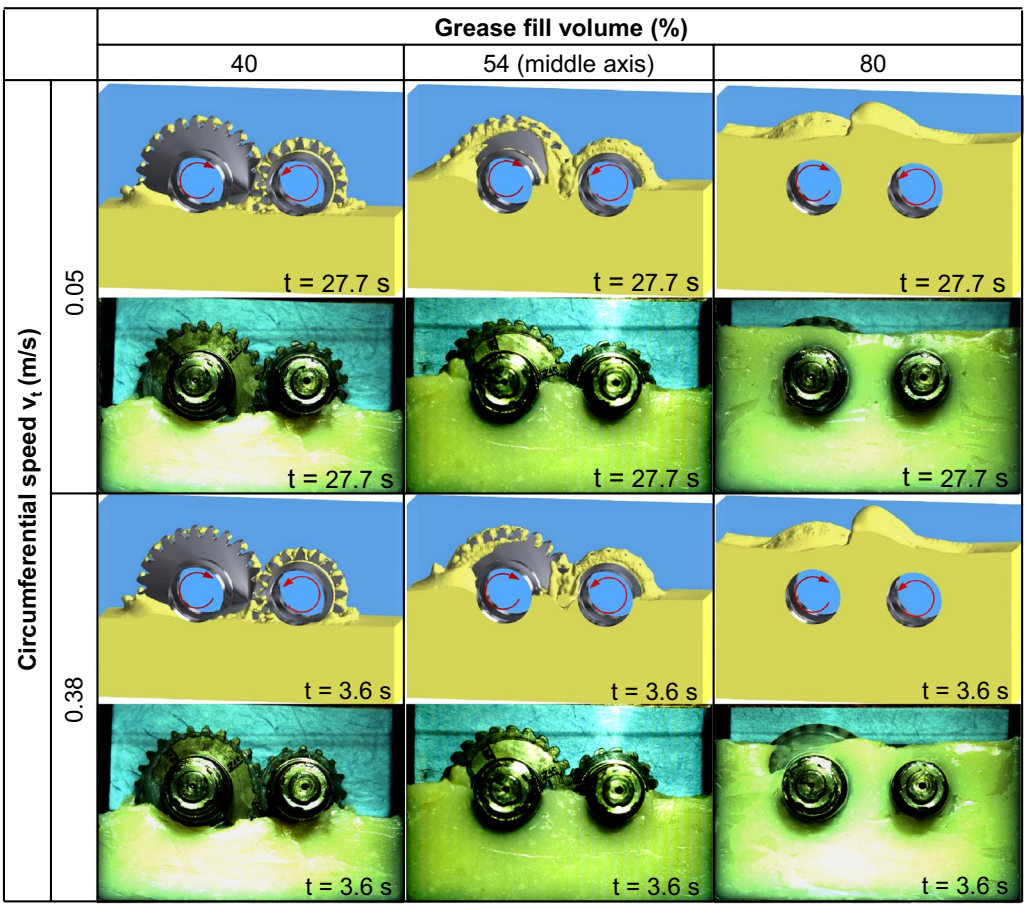

Figure 7 Simulated and recorded grease distribution for circumferential speeds v_t of 0.05 m/s and 0.38 m/s and grease fill volumes of 40%, 54% and 80% after four wheel rotations

the simulation results are illustrated in a slightly angled view to improve information transfer.

The amount of grease around the circumference of the gears clearly increases with increasing grease fill volume. The influence of circumferential speed v_t is subordinate compared to the influence of grease fill volume. Although the circumference of both pinion and wheel has become more uniformly covered with grease after four wheel rotations for all fill volumes, a quasi-stationary state has not been reached (Section 5.3).

The simulated degree of grease coverage of gears correlates qualitatively well with the high-speed camera recordings. For the grease fill volume of 80%, the bead above the gear mesh already observed after three-quarter wheel rotation in Figure 6 is not observed experimentally. The artifact may be related to some deviation between the measured and predicted values for the Bingham model (Figure 4). But also numerical inaccuracies originating from the remeshing process are possible.

Figure 8 quantifies the simulated grease fraction and Figure 9 the associated shear rate. The front view relates to the cumulated information over the tooth width of 14 mm, whereas the side view relates to a cross section through the middle of the wheel. It can be clearly seen that the rotating gears influence the grease sump only locally around the gears. This is illustrated by the shear band around the gears in Figure 9.

For the fill volume of 40%, the grease fraction around the circumference of the gears is low and shear band is very close to the tip diameter of pinion and wheel. For the fill volume of 54%, the grease fraction around the circumference of the gears as well as the diameter of the shear band increases. However, the grease dragged along the circumference is not enough to form a full circulating loop around the gears again leading to a widely separated rotation of the gears from the grease sump. For the grease fill volume of 80%, the grease fraction around the circumference and the diameter of the shear band is highest. The tooth gaps of both pinion and wheel are almost fully filled with grease. A circulating grease flow around the gears is present.

The observed grease flow phenomena for the different grease fill volumes can result in the different lubrication mechanisms found in literature (Section 2).

5.3 Grease Fraction around Gears

Based on Figure 8, Figure 10 shows the evaluated grease fraction around the pinion and wheel over the number of wheel rotations. Thereby, the fluid volume between the gear surface and an enveloping surface with a distance of 1 m_n (4.5 mm) in axial direction from the gear front surfaces and in radial direction from the gear tip diameters is evaluated.

For the grease fill volume of 54%, a clear bulbous trend of the grease fraction is visible for each wheel rotation. During the first half wheel rotation, the increase of grease fraction is referred to limited grease flow to the evaluated fluid volume. During the second half wheel rotation, grease carried out from the sump reaches the gear mesh (Figure 6) and is partly squeezed out reducing the grease fraction in the evaluated fluid volume. As the number of rotations increases, the bulbous trend becomes less

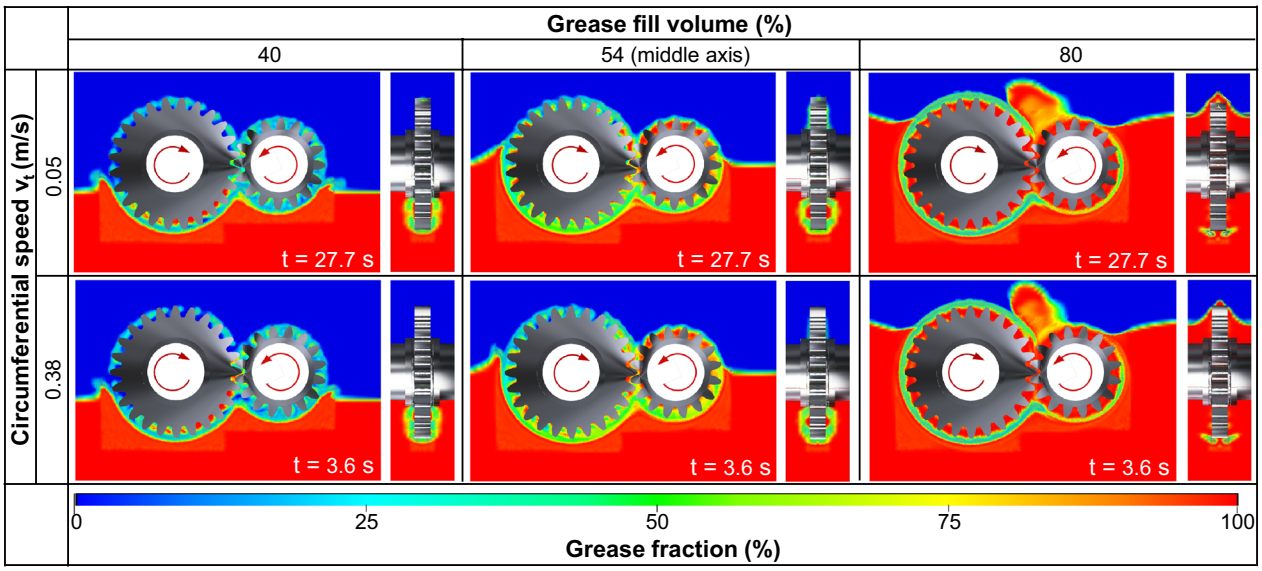

Figure 8 Simulated grease fraction from the front view (over tooth width) and side view (cross section though middle of wheel) of the gearbox for the considered operating points after four wheel rotations

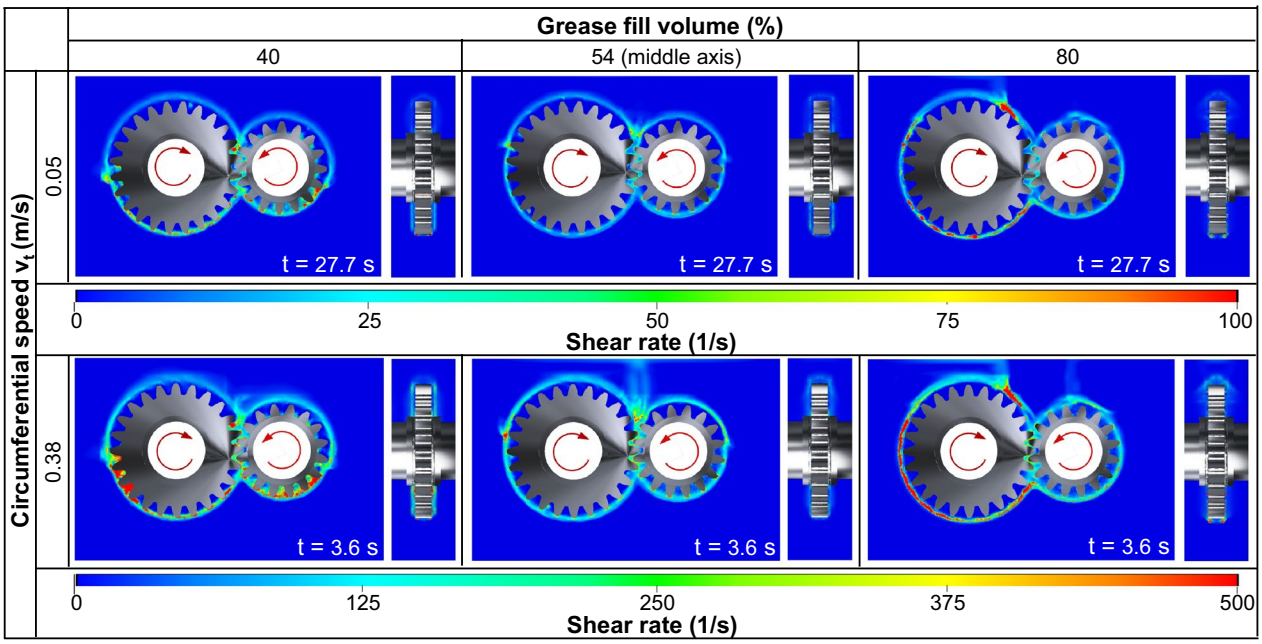

Figure 9 Simulated shear rate from the front view (over tooth width) and side view (cross section though middle of wheel) of the gearbox for the considered operating points after four wheel rotations

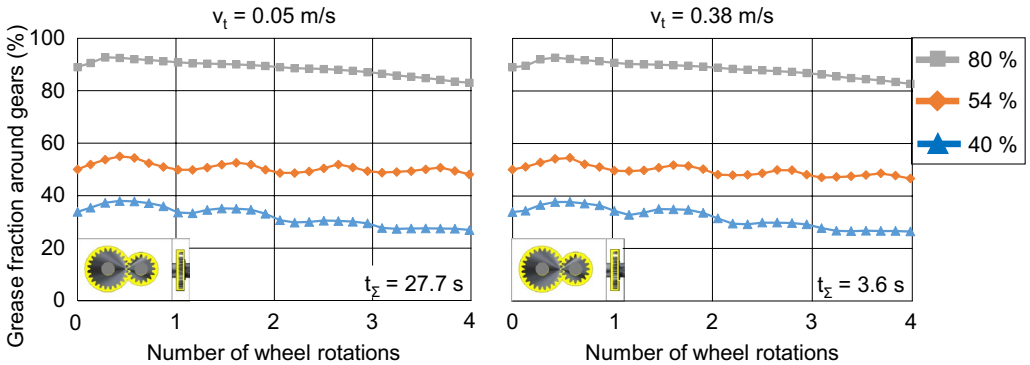

Figure 10 Simulated grease fraction evaluated in a fluid volume around the pinion and wheel over the number of wheel rotations for the considered operating conditions

pronounced, as the grease distribution becomes more homogenized over the circumference of the gears (Figure 7). For the fill volume of 40%, the behavior of the grease fraction over wheel rotations is similar. For the fill volume of 80%, the bulbous trend of the grease fraction is not pronounced, since the grease distribution over the circumference of the gears is almost homogeneous before start-up.

The mean grease fraction decreases over the number of wheel rotations for all fill volumes. This will continue until a quasi-stationary state is reached, which is not the case after the four wheel rotations simulated. Table 5 shows the percentage reduction of the grease fraction around the gears for the grease fill volumes of 40% and 80%. Thereby, the mean grease fraction over the first and fourth wheel rotation was evaluated.

The results show that the percentage reduction of the grease fraction around the gears is much higher for a grease fill volume of 40% compared to 80%. This is in accordance with the observed grease flow phenomena in Section 5.2. When comparing the circumferential speeds the trends and values of the evaluated grease fractions are very similar. This confirms the observations in Section 5.2 and shows that for the circumferential speeds considered the gear-grease interaction per rotation is very similar. The centrifugal force has no remarkable

Table 5 Percentage reduction of grease fraction around pinion and wheel over four wheel rotations

Grease fill volume (%)	Circumferential speed v_t	
	0.05 m/s	**0.38 m/s**
40	− 23.5%	− 24.7%
80	− 6.9%	− 7.0%

impact on the grease distribution. The behavior can be different for higher circumferential speeds.

6 Conclusion

Within this study, a finite-volume based CFD model of a single-stage gearbox lubricated with an NLGI 1-2 grease was built to investigate the fluid flow. It was found that the rotating gears influence the grease sump only locally around the gears, which was illustrated by shear bands. The backflow of grease to gear rotation areas in the sump was limited. A high grease fill volume of the gearbox improved the gear-grease interaction and the grease fraction around the circumference of the gears increased. Hence, a circulating grease flow around the gears can be beneficial for lubrication and heat transfer. Contrary to the considered fill volumes, the considered circumferential speeds showed no significant influence on the grease flow behavior. The simulated grease distributions showed good accordance with high-speed camera recordings. Further studies can focus on a larger spread of operating conditions to investigate the correlation between grease flow phenomena and the lubrication mechanisms channeling and circulating reported in literature systematically.

Abbreviations

A_f	Border area of control volume
a	Center distance in mm
BH	Bingham
b	Tooth width in mm
CV	Control volume
D_Φ	Diffusive flow
d_a	Tip diameter in mm
F	Exterior force in N
FV	Finite-volume
F_Φ	Convective flow
f	Centroid of border of control volume
g	Gravity in m/s^2
h	Specific enthalpy in J/kg
i_{12}	Gear ratio
L	Characteristic length in mm
m	Consistency index
m_n	Normal module in mm
$\dot{m}_{pq}$	Mass flow rate phase 1 to phase 2
$\dot{m}_{qp}$	Mass flow rate phase 2 to phase 1
n	Flow index | Rotational speed in r/min | time step
P	Center of control volume
p	Phase 1
r_p	Pitch radius in mm
Q_Φ	Sources
q	Phase 2
q'''	Specific heat in J/(kg·K)
Re	Reynolds number
S_{α_q}	Source term of phase 2 in kg/s
SF	Surface of control volume
U_f	Volume flow rate in m^3/s
U	Flow velocity in m/s
u	Flow velocity in m/s
V	Volume of control volume in m^3
v_t	Circumferential speed in m/s
x	Addendum modification coefficient
z	Number of teeth
α	Volume fraction
a_n	Pressure angle in °
Γ	Diffusion coefficient
$\dot{\gamma}$	Shear rate in 1/s
Δ	Laplace operator
δ t	Time interval in s
η	Dynamic viscosity in mPas
ρ	Density in kg/m^3
τ	Shear stress in Pa
τ_0	Yield stress in Pa
Φ	Arbitrary state variable
∇	Nabla operator
ν	Kinematic viscosity in mm^2/s
ω	Angular speed in rad/s
$\frac{\partial}{\partial t}$	Partial derivation of time

Acknowledgements

The authors would like to thank Dr. Gerd Dornhöfer and Dr. Alexander Elter from Robert Bosch GmbH for supporting with rheological measurements and modeling of the considered grease.

Author contributions

Conceptualization: HL and TL; methodology: HL and FD; investigations: HL and FD; data curation: HL and FD; visualization: HL and FD; writing—original draft preparation: HL and FD; writing—review and editing: HL and TL; formal analysis: HL and TL; supervision: TL; funding acquisition: TL and KS; project administration: TL and KS; resources: KS. All authors have read and agreed to the published version of the manuscript.

Authors Information

Hua Liu, born in 1988, was a doctoral candidate at *Gear Research Center (FZG) of the Technical University of Munich (TUM), Germany*, until 2021. He received his master degree from *TUM, Germany*, in 2014 and is currently finishing his doctoral thesis.

Florian Dangl, born in 1997, was a bachelor and master student at *Gear Research Center (FZG) of the Technical University of Munich (TUM), Germany*. He received his master degree from *TUM, Germany*, in 2022.

Dr.-Ing. Thomas Lohner, born in 1987, is currently head of the department EHL-Tribological-Contact and Efficiency at the *Gear Research Center (FZG)* of the *Technical University of Munich (TUM), Germany*. He received his doctoral degree from *TUM, Germany*, in 2016.

Prof. Dr.-Ing. Karsten Stahl, born in 1969, is currently head of *Gear Research Center (FZG) of the Technical University of Munich (TUM), Germany*. He received his doctoral degree from *TUM, Germany*, in 2000.

Funding

Supported by the German Research Foundation e.V. (DFG). The presented results are based on the research project STA1198/14-1.

Competing Interests

The authors declare no competing financial interests.

Received: 16 October 2020 Revised: 1 October 2022 Accepted: 3 January 2023
Published online: 24 February 2023

References

[1] T Goerz. Schmierfette auf Seifenbasis Zusammensetzung - Herstellung-Eigenschaften. *Tribologie und Schmierungstechnik*, 2009, 56(1): 32–39.
[2] H Schultheiss, J P Stemplinger, T Tobie, et al. Influences on failure modes and load carrying capacity of grease lubricated gears. *Gear Technology*, 2016: 42–47.
[3] DIN 51818: 1981-12, Schmierstoffe; Konsistenz-Einteilung für Schmierfette; NLGI-Klassen. 51818: 1981–12.
[4] H Liu, G Arfaoui, M Stanic, L Montigny, et al. Numerical modelling of oil distribution and churning gear power losses of gearboxes by smoothed particle hydrodynamics. *Proceedings of the Institution of Mechanical Engineers, Part J: Journal of Engineering Tribology*, 2018, 233(1), https://doi.org/10.1177/1350650118760626
[5] H Liu, T Jurkschat, T Lohner, et al. Determination of oil distribution and churning power loss of gearboxes by finite volume CFD method. *Tribology International,* 2017, 109, 346–354.
[6] H Liu, T Jurkschat, T Lohner., et al. *Numerical modeling and validation of oil distribution and churning losses in gearboxes*. 6th World Tribology Congress 2017, Beijing, China, 2017.
[7] H Liu, T Jurkschat, T Lohner, et al. Detailed investigation on the oil flow in dip-lubricated gearboxes by finite volumen CFD method. *Lubricants*, 2018, 6(2): 47.
[8] H Liu, P Standl, M Sedlmair, et al. Efficient CFD simulation model for a planetary gearbox. *Forschung im Ingenieurwesen*, 2018, 82: 319–330.
[9] F Concli. Numerical modelling of the churning power losses of gears: An innovative 3D computational tool suitable for planetary gearbox simulation. *Tribology International*, 2016, 103: 58–68.
[10] F Concli, C Gorla. Numerical modeling of the power losses in geared transmissions: Windage, churning and cavitation simulations with a new integrated approach that drastically reduces the computational effort. *Tribology International*, 2016, 103: 58–68.
[11] F Concli, C Gorla. Numerical modeling of the churning power losses in planetary gearboxes: An innovative partitioning based meshing methodology for the application of a computational effort reduction strategy to complex gearbox configurations. *Lubrication Science*, 2017, 29(7): 455–474.
[12] T Kvist. *Oil splashing simulation using CFD*. Trollhättan, Schweden, 2012.
[13] C Klier, L Berger, K Stock. New prospects for oil New prospects for oil flow simulation in rotating spur-gear systems. *International Conference on Gears*, Garching, Germany, October 7, 2015.
[14] L G Westerberg, E Höglund, C Sarkar. Modelling and experimental validation of grease flow. *Eurogrease Magazine*, 2016, 4: 17–32.
[15] L G Westerberg, C Sarkar, J F Lladós, et al. Lubricating grease flow in a double restriction seal geometry: A computational fluid dynamics approach. *Tribology Letters*, 2017, 65: 82.
[16] K P Gertzos, P G Nikolakopoulos, C A Papadopoulos. CFD analysis of journal bearing hydrodynamic lubrication by Bingham lubricant. *Tribology International*, 2008, 41(12): 1190–1204.
[17] J G Yoo, K W K Kim. Numerical analysis of grease thermal elastohydrodynamic lubrication problems using the Herschel-Bulkley model. *Tribology International*, 1997, 30(6): 401–408.
[18] T Nogi, M Soma, D Dong. Numerical analysis of grease film thickness and thickener concentration in elastohydrodynamic lubrication of point contacts. *Tribology Transactions*, 2020, 63(5): 924–934.
[19] M N Mastrone, F Concli. CFD simulation of grease lubrication: Analysis of the power losses and lubricant flows inside a back-to-back test rig gearbox. *Journal of Non-Newtonian Fluid Mechanics*, 2021, 297: 104652.
[20] K Fukunaga. Allowable surface durability in grease lubricated gears. *Tribology Transactions*, 1988, 31(4): 454–460.
[21] M Hochmann. *Zahnradtragfähigkeit bei Schmierung mit Getriebefließfetten*. Munich: Technical University of Munich, 2011.
[22] J P Stemplinger. *Tragfähigkeit und Wirkungsgrad von Stirnradgetrieben bei Schmierung mit hochviskosen Fluiden und Fetten NLGI 0, 1 und 2*. Munich: Technical University of Munich, 2013.
[23] J P Stemplinger, K Stahl, B Hoehn, et al. *Analysis of lubrication supply of gears lubricated with greases NLGI 1/2 and the effects on load-carrying capacity and efficiency*. 5th World Tribology Congress - WTC 2013, September 8-13, 2013: 1181–1183
[24] H Schultheiss, T Tobie, K Stahl. *Wear load carrying capacity of gears in small size transmissions with lubrication using high consistency grease*. DGMK-Forschungsbericht 766, Deutsche Wissenschaftliche Gesellschaft für Erdöl, Erdgas, 2016.
[25] B J Siewerin, A Dobler, T Tobie, et al. *Applicability of an oil based calculation approach for wear risk and wear lifetime to grease lubricated gear pairings*. ASME 2019 International Design Engineering Technical Conferences and Computers and Information in Engineering Conference, Anaheim, USA, August 18-21, 2019. https://doi.org/10.1115/DETC2019-97439
[26] D Fischer, G Jacobs, A Stratmann, et al. Effect of base oil type in grease composition on the lubricating film formation in EHD contacts. *Lubricants*, 2018, 6(2): 32.
[27] D Fischer, H Mues, G Jacobs, et al. Effect of over rolling frequency on the film formation in grease lubricated EHD contacts under starved conditions. *Lubricants*, 2019, 7(2): 19.
[28] R P Chhabra, J F Richardson. *Non-newtonian flow and applied rheology - Engineering applications*. 2nd ed. Oxford: Elsevier Science, 2008.
[29] E Maier, T Lohner, K Stahl, K. Tribologisches Verhalten kurzfaserverstärkter Polyamide. Forschungsvereinigung Antriebstechnik e.V.: Frankfurt am Main, Germany, 2022.
[30] R Schwarze. *CFD-Modellierung: Grundlagen und Anwendungen bei Strömungsprozessen*. Heidelberg: Springer, 2013.
[31] D Zhang, C Jiang, D Liang, et al. A refined volume-of-fluid algorithm for capturing sharp fluid interfaces on arbitrary meshes. *Journal of Computational Physics*, 2014, 274: 709–736.
[32] M Ehrentraut. *Numerische Untersuchungen zur Mischgüte beim Rühren von viskoplastischen Fluiden - Strömungssimulation für die Analyse von gerührten rheologisch komplexen Fluiden*. Wiesbaden: Springer Spektrum, 2016.
[33] R Courant, K Friedrichs, H Lewy. Über die partiellen Differenzengleichungen der mathematischen Physik. *Mathematische Annalen*, 1928, 100: 32–74.
[34] ISO, *FZG test method A/8,3/90 for relative scuffing load-carrying capacity of oils*. 14635-1, 2000.